# Nanoscale imaging of the electronic tunneling barrier at a metal surface

G. R. Condon[a] and J. A. Panitz
*Department of Physics and Astronomy, University of New Mexico, Albuquerque, New Mexico 87131*

(Received 19 September 1997; accepted 7 November 1997)

A photometric field-emission electron microscopy technique is described by which the spatial structure of the surface electronic tunneling barrier can be mapped with nanometer resolution. The technique involves performing a Fowler–Nordheim analysis on luminosity data extracted from a set of digitized field-emission images taken over a range of voltages. This approach is equivalent to older probe-hole methods, but with greatly improved spatial resolution and data accumulation rate. Virtual probe holes of arbitrary size and shape can be constructed by integrating over subregions in the field-emission images. Performance of a system utilizing this technique is demonstrated by measuring the work functions of the (111) and (100) crystallographic planes of a clean tungsten field emitter. Applications of this technique to adsorption phenomena and field-emission display technology are also discussed. © *1998 American Vacuum Society.* [S0734-211X(98)06601-3]

## I. INTRODUCTION

Developed in the 1930s, field-emission microscopy,[1,2] is one of the oldest techniques of modern surface analysis. In a field-emission electron microscope (FEEM), electrons are emitted from the surface of a metal cathode for electric-field strengths approaching 1 V/Å, and are imaged on a distant anode coated with a cathodoluminescent material. The spherical FEEM,[2] characterized by a sharp wire cathode and a spherical anode, offers the lowest image distortion as well as the most convenient geometry for creating large-field enhancements at the emitter surface. It can produce magnifications on the order of $10^6$ (~2 nm resolution) due to the divergence of the electric-field lines.[2–4] The pattern of electron emission imaged in a FEEM depends primarily on the crystallographic structure of the surface as this defines the potential-energy barrier and the local supply of tunneling electrons. The height of the potential barrier is described by the intrinsic work function, the width by the applied field strength, and the supply of tunneling electrons by the local density of states (LDOS) at the surface. In this article, we describe a derivative imaging technique for the FEEM by which nanoscale features in the surface potential-energy barrier can be resolved independently of the surface LDOS.

The field-emission process, first observed in the 18th century,[5] was intensely scrutinized in the early 20th century when it came into prominence as a demonstration of the then-new theory of quantum-mechanical tunneling.[6] By describing the cathode as a one-dimensional Fermi sea of electrons separated from the vacuum by a triangular potential barrier with height equal to the work function of the field-free surface and width determined by the strength of the applied field, Fowler and Nordheim[7,8] derived a relationship between the emitted current density and the applied field of the following form:

$$J \propto F^2 \exp\left(\frac{-\phi^{3/2}}{F}\right), \qquad (1)$$

where $J$ is the field-emission current density, $F$ is the electric-field strength at the surface, and $\phi$ is the work function. If the field can be written in the form $F = V/kR$, where $kR$ is an effective local radius of curvature, then the Fowler–Nordheim equation may be linearized by the following change of variables:

$$\ln\left(\frac{I}{V^2}\right) = -\phi^{3/2} kR \times \left(\frac{1}{V}\right) + \text{const.} \qquad (2)$$

The slope of $\ln(I/V^2)$ vs $(I/V)$ depends only on the form of the tunneling barrier, as defined by $\phi$ and $kR$, and not on the surface LDOS. Measurements of this ''Fowler–Nordheim slope'' have been widely used to determine the work functions of surfaces with known geometries, the geometries of surfaces with known work functions, and the relative work functions of surfaces before and after various modifications.[9]

Because the emission from a real cathode is actually a superposition of emissions from a variety of distinct crystallographic faces, several techniques have been developed to measure current–voltage data from small regions of the emitter surface independently. The most accepted technique for this purpose is the use of the ''probe-hole'' FEEM developed by Müller in 1943.[10] In a probe-hole FEEM, a physical aperture is placed between the cathode and a current measuring anode so that only emission from the region of interest is collected. Because of the difficulties in positioning a physical probe hole in vacuum, this technique was quickly modified so that current–voltage data could be extracted from luminosity measurements taken from a phosphor coated anode using a photodetector located external to the vacuum system.[11–13] Despite strenuous criticism of this approach,[10,14,15] work-function measurements of the various crystal faces of tungsten taken with this ''photometric probe-hole'' technique have proven to be of comparable accuracy as physical probe-hole measurements from the same period. Both physical and photometric probe-hole techniques have been used almost exclusively with a single probe hole at a time and have, therefore, been limited to providing only one channel of data. Today, the availability of inexpensive

[a]Electronic mail: gcondon@unm.edu

charge coupled device (CCD) cameras and digital frame grabbers has made it feasible to construct a multichannel photometric probe-hole FEEM.[16,17] In this article, we describe a technique by which a multichannel photometric probe-hole FEEM can be used to independently determine the Fowler–Nordheim characteristics for each pixel in a set of digitized field-emission images taken over a range of voltages. Our technique, which we call ''PhotoFEEM'', extends traditional Fowler–Nordheim analysis by providing a spatially resolved map of the surface tunneling barrier on a nanometer scale. From this map, Fowler–Nordheim characteristics can be extracted from any region of the emitter's surface. We demonstrate the utility of this technique by measuring the work functions of the (111) and (100) crystal faces of a tungsten field emitter. Our measurements are in good agreement with work functions obtained with other methods and display spatial structure in the surface tunneling barrier, which to the best of our knowledge has not been previously observed. We also discuss other potential applications of this technique including imaging the tunneling barriers associated with molecular adsorbates and the spatial characterization of emitter characteristics in field-emission displays (FEDs).

## II. CONCEPT

In a PhotoFEEM experiment, a three-dimensional data cube is constructed from a stack of two-dimensional FEEM images taken over a range of voltages. The FEEM images are gathered with an array photodetector, such as a CCD camera, and digitized to allow for the subsequent extraction of virtual probe holes with a computer. Probe holes of arbitrary size and shape can be built up as collections of individual pixels limited only by the size of an individual pixel. Luminosities, suitable for Fowler–Nordheim analysis, are obtained by simply summing the pixel values within the virtual probe hole for each voltage (Fig. 1). Because the parameter of interest in a Fowler–Nordheim analysis is the slope of $\ln(I/V^2)$ vs $(I/V)$, the luminosity data need only be proportional to the incident currents for the method to be identical to a traditional probe-hole experiment. In other words, if the luminosities are proportional to the incident currents, the constant of proportionality, $c$, appears as an additive constant in Eq. (2):

$$\ln\left(\frac{L}{V^2}\right)=\ln\left(\frac{I}{V^2}\right)+\ln(c), \tag{3}$$

and, therefore, does not affect the Fowler–Nordheim slope. As long as this condition is satisfied, a Fowler–Nordheim analysis can be performed on each pixel in a set of digitized FEEM images. Even with a commercial grade CCD camera, this can be equivalent to over $10^5$ traditional probe-hole measurements taken in parallel. The ultimate resolution of such a system is limited by the resolution of the FEEM image ($\sim 2$ nm),[2–4] thereby allowing nanometer resolution imaging of the surface tunneling barrier.

We note that barrier maps can also be constructed from measurements of current versus electrode separation data in

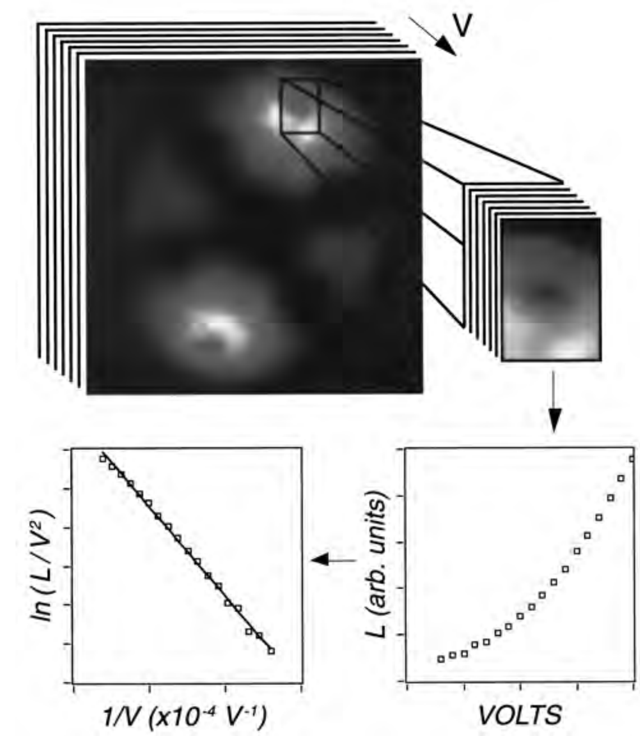


FIG. 1. Schematic illustration of the PhotoFEEM concept. (Clockwise from upper left) a series of FEEM images are taken over a range of voltages, an arbitrary ''probe hole'' is extracted from the set of images, luminosities are obtained by integrating over the probe hole for each voltage, and a Fowler–Nordheim analysis is performed on the transformed data $\ln(L/V^2)$ vs $(1/V)$.

the scanning tunneling microscope (STM). However, the interpretation of the STM map is not straightforward. The barrier width is changed in the STM and the FEEM, respectively, by varying the interelectrode spacing or the magnitude of the applied electric field. Accurate work functions, consistent with other measurement techniques, can be extracted directly from PhotoFEEM data. However, work functions measured from STM current versus electrode spacing data are, typically, lower than accepted values due to tip–substrate work-function averaging and geometrical effects related to the projection of $ds$ along the surface normal.[18,19] Limitations to the applicability of the PhotoFEEM technique arise from the fact that the samples must be formed into or deposited on sharp tips ($\sim 1$ $\mu$m radius of curvature) and must withstand the mechanical stresses that result from the application of strong electric fields ($\sim 1$ V/Å).

Any FEEM can be used with the PhotoFEEM technique so long as the raw image data is processed appropriately. In most situations, the image processing reduces to three simple steps: normalization of exposure times, ''dark subtraction'' of the noise background in each image, and correction for the response of the imaging system. The normalization of exposure times is required by the limitations in dynamic range and resolution of any digital imaging system. Because there are only a finite number of gray levels in a digital image, as determined by the bit depth of the analog-to-digital conversion (ADC) stage, the greatest amount of data is obtained by integrating the image until the full dynamic range of the ADC is filled. Obviously, this integration time depends on the brightness of the image. To facilitate comparison between images taken at different tunneling voltages, and therefore different image brightnesses, each image must be normalized to a fixed exposure length. The dark subtraction step is needed because of the nonzero noise contribution from the electronics in the imaging system. This effect is easily negated by the subtraction of a dark image taken with no field-emission pattern present. It is important to note that this dark image, which contains only noise, must also be normalized to the same exposure time as the data images for the subtraction to be valid. Incorrect dark subtraction can lead to a pronounced nonlinearity in the plot of $\ln(L/V^2)$ vs $(I/V)$.

The final step in the processing is a correction for the response of the imaging system. The primary concern is the dependence of the luminous response of a phosphor on the mean kinetic energy of the incident electrons. In a conventional FEEM, the applied voltage that determines the tunneling current is also the accelerating voltage that imparts kinetic energy to the electrons *en route* to the anode. Therefore, as the tunneling bias is increased, the luminosity per unit current increases along with the tunneling current. In order to ensure a simple proportionality between current and luminosity, one must determine the luminosity per unit current of the phosphors as a function of incident electron energy. It has been found[20] that over large ranges in accelerating voltage (0.5–10.0 kV), the relationship between luminosity and current goes as $L/I = kV^n$ where $n$ is a constant, usually between 2 and 3, that depends on the type of phosphor, and $k$ is a constant of proportionality that depends on the units of $L$ and $I$. However, over the abbreviated voltage range (3–5 kV) used in our experiments, we demonstrated that the phosphor response can be adequately described as a linear function of voltage. In a FEEM with an acceleration stage that can be controlled independently of the tunneling bias, such as systems with gate electrodes or microchannel plates, this effect can be eliminated. In addition to the phosphor effect, the response of the imaging system is sensitive to the aperture size and reproduction ratio of the camera and possibly to the aging of the phosphors under electron bombardment. However, these effects can be minimized by maintaining a fixed geometry for the camera system and recalibrating the response of the system periodically.

## III. DESIGN AND OPERATION

Our prototype PhotoFEEM (Fig. 2) was designed to test the validity of using photometric data, in lieu of direct current measurements, in the Fowler–Nordheim analysis of field-emission experiments. We have demonstrated this in two ways: (1) by verifying that the Fowler–Nordheim slope determined from current measurements for the whole emitter could be reproduced from independently calibrated luminosity data, and (2) by measuring work functions for the (111) and (100) crystal planes of tungsten that are in good agreement with accepted values. The experiments were conducted using a commercial FEEM tube[21] consisting of a highly evacuated spherical glass bulb containing a tungsten field emitter and a phosphor screen. The tube was designed by Müller and reflects the form of his original microscope.[2] A high-voltage power supply[22] provided tunneling bias, and a picoammeter[23] was used to measure the integrated tunneling current incident at the anode. Images were acquired from a CCD camera,[24] then summed and digitized by a stand-alone image processing unit.[25] Summing of individual video frames continued until the maximum pixel value of the digitizer was reached (4096 levels, $512\times512$ pixels). Afterwards, the data images were transferred to a computer[26] for subsequent analysis. The data acquisition was controlled by computer[26] with images and current measurements taken in 15–35 V increments over a range of voltages between 3 and 5 kV (currents between 10 nA and 1 $\mu$A). The computer control program, and all the subsequent analysis codes, was developed in-house with the LABVIEW development environment.[27]

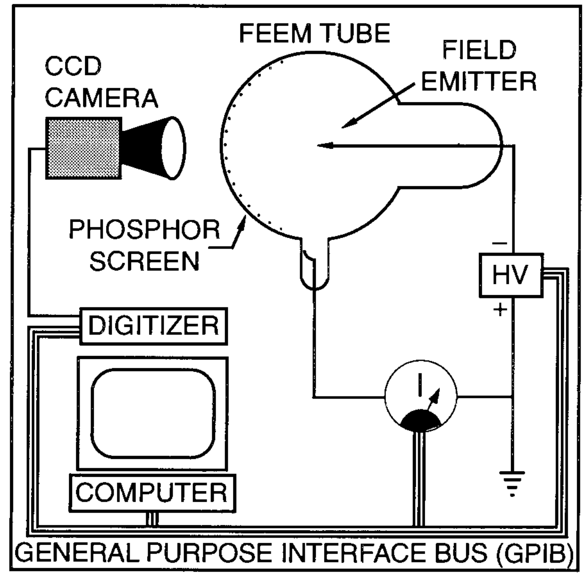


FIG. 2. Schematic illustration of the prototype PhotoFEEM apparatus.

After data collection, raw luminosities were extracted from the digitized images. As described previously, the luminosities were processed in a series of three steps; normalization, dark subtraction, and response correction prior to the calculation of any barrier maps. In the first experiment, the response of the imaging system was calibrated with a separate vacuum system in which a similar P1 phosphor ($Zn_2SiO_4$:Mn) screen was illuminated by the electron emission from a nude Bayard–Alpert ionization gauge as intensified by a pair of microchannel plates (gain $\sim 10^6$). The geometry of the imaging system in the FEEM experiments was duplicated as closely as possible and the kinetic energy of the electrons was controlled by varying the accelerating voltage between the channel plates and the phosphor screen. The phosphor response was found to be linear between 3 and 5 kV. For the sake of comparison with the anode current

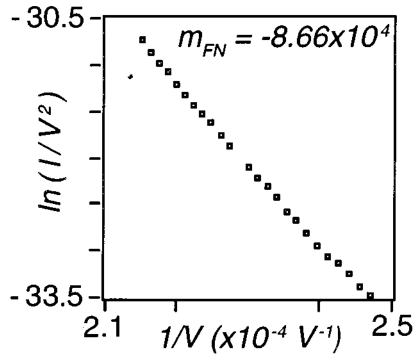


FIG. 3. Fowler–Nordheim plot of the anode current data from the first proof-of-concept experiment.

data, the raw luminosities were extracted from an aperture encompassing the entire image plane. The current–voltage and processed-luminosity–voltage data for this experiment, shown in Figs. 3 and 4, are both clearly linear in the Fowler–Nordheim coordinates. A comparison of slopes for best-fit straight lines to the data reveals an agreement of better than 2%. The small disagreement between the two Fowler–Nordheim slopes is probably due to slight differences between the experimental apparatus and the system used for calibration.

In the second experiment, we calculated work functions for the (111) and (100) crystal faces of tungsten from PhotoFEEM luminosity data. We decided to perform this experiment because of the presence of factors (such as screen non-uniformity and excessive scattered light)[10,14,15] that could prevent extraction of reliable data from small regions and would not have been detected in the first experiment. The (111) and (100) planes were chosen because one is bright and one is dark, respectively, and they are easily located. For this experiment, instead of using the independent phosphor calibration, which was determined for a different screen, we opted to self-calibrate the data by measuring the phosphor response, $L/I$ vs $V$, from the full image data. Clearly, cali-

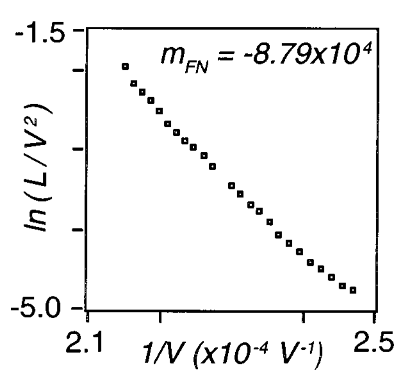


FIG. 4. Fowler–Nordheim plot of the processed luminosity data from the first proof-of-concept experiment.

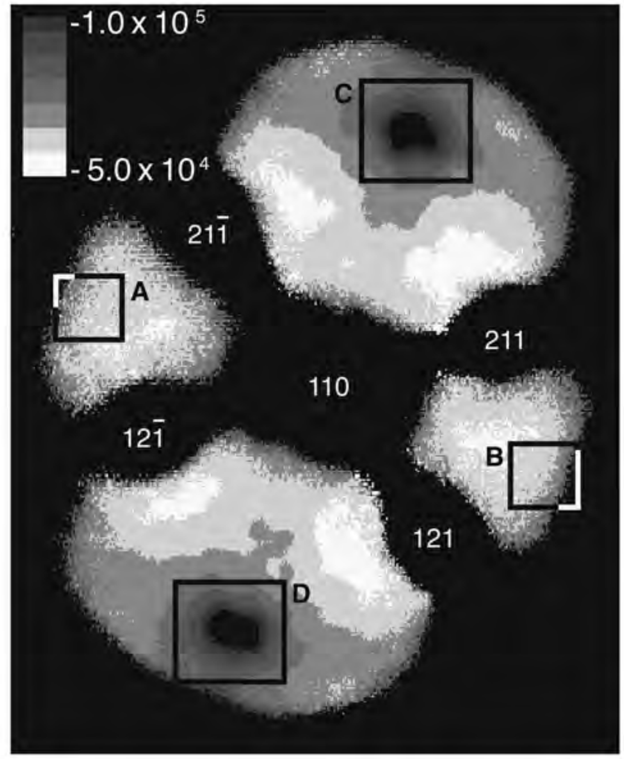


FIG. 5. PhotoFEEM barrier map of the clean tungsten field emitter from the second proof-of-concept experiment. Compare with the FEEM image included in Fig. 1. The (110) and {211} crystallographic planes are labeled. The {111} apertures, A and B, and the {100} apertures, C and D, are outlined and labeled.

brating with this response function trivially enforces the condition that the luminosity and current data yield the same Fowler–Nordheim slopes at the full image level. After the luminosities were fully processed, a pixel-by-pixel ''barrier map'' of the Fowler–Nordheim slopes across the surface of a clean tungsten field emitter was constructed (Fig. 5). Often times there is insufficient signal in a single pixel, especially at low voltages and on ''dark'' crystal planes, to extract a reliable luminosity. Pixels that contain only fluctuations in the noise background yield negative luminosities after dark subtraction approximately half the time. Therefore, in order to exclude any questionable measurements, Fowler–Nordheim slopes were calculated only for pixels that had, after processing, a positive luminosity for each voltage in the data set. This stringent rejection criterion insures that any structures seen in the barrier map are not artifacts due to noisy measurements or least-square fitting to small data sets.

Apertures enclosing the (111) and (100) planes were constructed and integrated Fowler–Nordheim plots were made for these apertures (Fig. 6). The luminosities were extracted from the raw image data and, after processing, were appropriately positive for all voltages in the data set. Assuming that the magnification and radius of curvature are roughly constant across the surface, the ratio of Fowler–Nordheim slopes, $m_1$ and $m_2$, for two subregions of the surface is related to the relative work functions $\phi_1$ and $\phi_2$ as

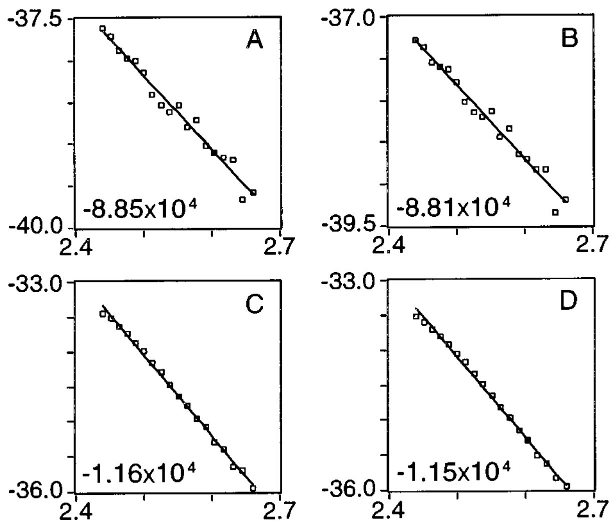


FIG. 6. PhotoFEEM Fowler–Nordheim plots, $\ln(L/V^2)$ vs $1/V \times(\times 10^{-4} V^{-1})$, for the four apertures shown in Fig. 6. The Fowler–Nordheim slope of the best-fit straight line is indicated in the bottom left corner of each plot.

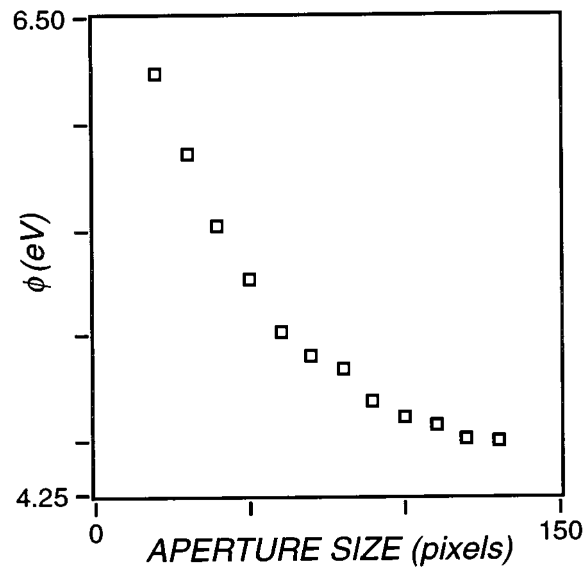


FIG. 7. Work function vs aperture size for a square aperture centered over the upper (100) plane shown in Fig. 6.

$$\frac{m_1}{m_2}=\left(\frac{\phi_1}{\phi_2}\right)^{3/2} \rightarrow \phi_1=\left(\frac{m_1}{m_2}\right)^{2/3} \phi_2 . \tag{4}$$

Work functions were calculated for the (111) and (100) planes by comparison with the Fowler–Nordheim slope calculated for the entire emitter ($m_{\mathrm{FN}}=-9.95\times10^4$ V). This slope was assumed to correspond to a known mean work function of 4.55 eV for clean tungsten.[28,29] The work functions calculated in this fashion are 4.21 eV for (111) and 4.97 eV for (100), which agree well with the accepted values[28,29] of 4.47 eV for (111) and 4.63 eV for (100) to $-6\%$ and $+8\%$, respectively. This level of agreement is as good as can be expected considering that no corrections are made for variations in the electric-field strength across the surface.[11] Because of the symmetry of the (110)-oriented projection of a cubic lattice,[30] there are two occurrences each of {100} and {111} type planes present in the data set (Fig. 5). Work functions were calculated independently, with identical apertures, for both instances of each plane and the two values agree to better than 1% in both cases.

## IV. DISCUSSION

The two greatest difficulties with the PhotoFEEM method are ensuring a uniform luminous response across the images, both spatially and with respect to voltage, and eliminating scattered light from the dark regions of the field-emission pattern.[10,14,15] The uniformity with respect to voltage is ensured by the calibration, and the agreement between work functions for the two pairs of identical planes indicates excellent spatial uniformity across the phosphor screen. The presence of scattered light in the dark regions can cause anomalously low work-function measurements[11] that are approximately equal to the intensity weighted mean work function for the entire emitter (i.e., the source of the scattered light). The fact that we measured a work function for the dark (100) plane well in excess of the mean work function for the emitter indicates that scattered light is not the primary source of signal in the dark regions. In fact, if we shrink the (100) aperture down to only the darkest spot, we obtain a work function for (100) in excess of 6 eV (Fig. 7). Some regions such as the (110) plane are sufficiently dark to preclude any measurement within the limited sensitivity of our prototype apparatus. The very high work function for the darkest part of (100) is consistent with Müller's observations of ion production from aluminum, but not copper, evaporated from a hot, polycrystalline tungsten wire.[15] However, there are few direct measurements to indicate a work function in this range for any tungsten surface.[28,29] The sensitivity of the work function on aperture size raises serious questions about how best to choose the measurement region in this type of experiment. However, since our purpose in these experiments was to reproduce previous measurements, we chose an aperture size that we believe is representative of the size of physical apertures used in similar experiments.[15] Nevertheless, the dependence of the work function on aperture size is interesting, although perhaps not surprising, and is most likely due to the apparently continuous variation of the work function across the surface in the absence of a detailed correction for the surface electric-field distribution. We note that, to the best of our knowledge, this effect has not been observed in previous experiments[11,13,15] and is only accessible in this work due to the novelty of the PhotoFEEM technique.

The PhotoFEEM can be used in any experiment that currently relies on traditional probe-hole methods. Furthermore, because the barrier map of a surface is, to a good approximation, independent of the surface LDOS (while the direct FEEM image is not), comparative studies using both tradi-

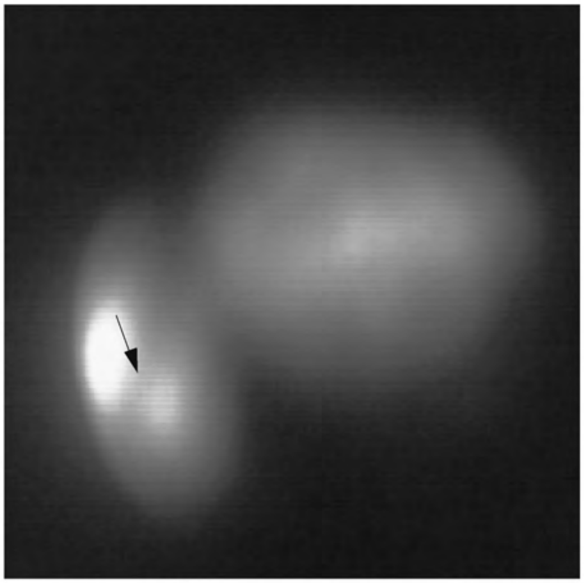

FIG. 8. FEEM image of a single Spindt-type microfabricated field emitter. The cleft discussed in the text is indicated with an arrow.

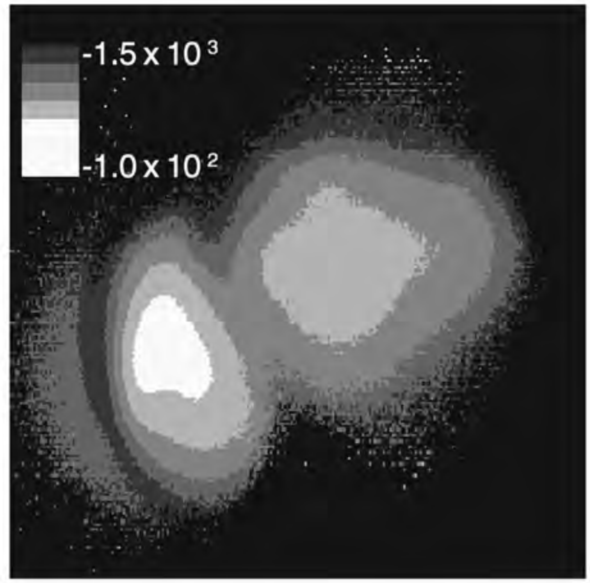


FIG. 9. PhotoFEEM barrier map of the cathode shown in Fig. 8.

tional FEEM and PhotoFEEM may be used to determine if the emission from a surface is limited by the local tunneling barrier or by the supply of tunneling electrons. As a demonstration, compare the image of the clean emitter in Fig. 1 to the barrier map in Fig. 5. The barrier map appears qualitatively similar to the corresponding FEEM image indicating that, over most of the surface, the tunneling current is primarily barrier limited. However, note that, while the brightness of the FEEM image reaches a maximum near the (100) plane and drops off monotonically towards the (211) plane, the barrier map indicates the opposite behavior—a work-function maximum near (100) and decreasing towards (211). This line passes through the series of $(11n)$ planes, where $n$ is an integer, with the (116) plane close to (100) and the (113) plane near (211).[30] The observation of conflicting behavior between the FEEM image and the PhotoFEEM barrier map is consistent with previous observations of greater emission from (116) as compared to (113),[14] even though (113) has a lower work function than (116).[28] This effect is too pronounced to be eliminated by adjusting for field variation, which is only a few percent effect, but more likely represents a situation where the emission from (113) is more limited by its supply of tunneling electrons than (116). Presently, we are using the PhotoFEEM technique to the characterize microfabricated cathode arrays for flat panel FEDs. In Figs. 8 and 9, we present a FEEM image and a PhotoFEEM barrier map for a single-tip molybdenum Spindt-type cathode.[31] For the most part, features present in the FEEM image are reflected in the barrier map indicating barrier limited tunneling. However, the absence in the barrier map of the smaller dark cleft in the FEEM image (see the arrow in Fig. 8) may indicate that the tunneling current in that region is supply limited. We are continuing to investigate these features in the barrier maps of microfabricated cathodes and their effects on emitter uniformity and lifetime.

## ACKNOWLEDGMENTS

The authors would like to thank Professors D. Dunlap and P. Schwoebel for many helpful discussions. This research was supported by a contract with SRI International of Menlo Park, California and by a graduate fellowship from the Center for Advanced Studies in the Department of Physics and Astronomy, University of New Mexico.

[1] R. P. Johnson and W. Shockley, Phys. Rev. **49**, 436 (1936).
[2] E. W. Müller, Z. Tech. Phys. (Leipzig) **11**, 412 (1936).
[3] R. Gomer, J. Chem. Phys. **20**, 1772 (1952).
[4] D. J. Rose, J. Appl. Phys. **27**, 215 (1956).
[5] C. Kleint, Prog. Surf. Sci. **42**, 101 (1993).
[6] For a review of this period, see R. O. Jenkins, Rep. Prog. Phys. **9**, 177 (1943).
[7] R. H. Fowler and L. W. Nordheim, Proc. R. Soc. London, Ser. A **119**, 173 (1928).
[8] L. W. Nordheim, Proc. R. Soc. London, Ser. A **121**, 626 (1928).
[9] R. Gomer, Surf. Sci. **299/300**, 129 (1994).
[10] E. W. Müller, Z. Phys. **120**, 261 (1943).
[11] M. K. Wilkinson, J. Appl. Phys. **24**, 1203 (1953).
[12] R. Gomer and D. A. Speer, J. Chem. Phys. **21**, 73 (1953).
[13] W. P. Dyke *et al.*, J. Appl. Phys. **25**, 106 (1954).
[14] E. W. Müller, Ergeb. Exakt. Naturw. **27**, 327 (1953).
[15] E. W. Müller, J. Appl. Phys. **26**, 732 (1955).
[16] M. F. H. van Tol *et al.*, Surf. Sci. **266**, 529 (1992).
[17] M. F. H. van Tol *et al.*, Surf. Sci. **266**, 214 (1992).
[18] G. Binnig and H. Rohrer, IBM J. Res. Dev. **30**, 355 (1986).
[19] G. Binnig and H. Rohrer, Surf. Sci. **126**, 236 (1983).
[20] W. B. Nottingham, J. Appl. Phys. **10**, 73 (1939).
[21] CENCO Part No. 55460U. Central Scientific Company, 3300 CENCO Parkway, Franklin Park, Illinois 60131.
[22] Model No. 225.20. Bertan High Voltage, 121 New South Road, Hicksville, NY 11801.
[23] Model No. 486 Picoammeter. Keithley Instruments Inc., 28775 Aurora Road, Cleveland, OH 44139.
[24] Model No. 4810 Monochrome CCD Camera. Cohu Inc., Electronics Division, Box 85623, 5755 Kearny Villa Road, San Diego, CA 92123.
[25] Model No. DS-20 Digital Image Memory/Processor. Quantex Corporation. No longer in business.
[26] Two separate computers were used in the experiments. For data acquisi-

tion, we used a Macintosh LCIII with a National Instruments (Ref. 27) GPIB interface card (Model No. LC-GPIB). For analysis, we used a Power Macintosh 8500/120. Apple Computer Inc., 1 Infinite Loop, Cupertino, CA 95014.
[27]National Instruments, 6504 Bridge Point Parkway, Austin, TX 78730-5039.
[28]H. B. Michaelson, J. Appl. Phys. **48**, 4729 (1977).
[29]V. S. Fomenko, *Handbook of Thermionic Properties* (Plenum, New York, 1966).
[30]E. W. Müller and T. T. Tsong, *Field Ion Microscopy: Principles and Applications* (Elsevier, New York, 1969).
[31]I. Brodie and C. A. Spindt, Adv. Electron. Electron Phys. **83**, 1 (1992).